Ferromagnetism in an Extended Three-Dimensional, Diamond-like Copper(II) Network: A New Copper(II)/1-Hydroxybenzotriazolato Complex Exhibiting Soft-Magnet Properties and Two Transitions at 6.4 and 4.4 K

Vassilis Tangoulis, Catherine P. Raptopoulou, Vassilis Psycharis, and Aris Terzis*

Institute of Material Science, NCSR Demokritos, 15310 Aghia Paraskevi Attikis, Greece

Konstantina Skorda and Spyros P. Perlepes*

Department of Chemistry, University of Patras, 26500 Patras, Greece

Olivier Cador and Olivier Kahn[†]

Laboratoire des Sciences Moléculaires, Institut de Chimie de la Matière Condensée de Bordeaux, 68 Avenue du Docteur A. Schweitzer, UPR CNRS 9048, 33608 Pessac, France

Evangelos G. Bakalbassis*

Laboratory of Applied Quantum Chemistry, Department of General and Inorganic Chemistry, Faculty of Chemistry, Aristotle University of Thessaloniki, P.O. Box 135, 54006 Thessaloniki, Greece

Received September 27, 1999

The use of the substituted benzotriazole ligand btaOH (1-hydroxybenzotriazole) in copper(II) chemistry has yielded a structurally and magnetically very interesting complex. The $[Cu_2(O_2CMe)_4(H_2O)_2]$/btaOH·H_2O/aqueous NH_3 (1:4:4, 1:3:3, 1:2:2) reaction system in MeOH gives dark brown-green $[Cu(btaO)_2(MeOH)]_n$ (**4**) in ∼80% yield. **4** crystallizes in the tetragonal space group $P4_32_12$ with (at 25 °C) $a = 9.915(1)$ Å, $b = 9.915(1)$ Å, $c = 14.715(2)$ Å, and $Z = 4$. The structure consists of a 3D, diamond-like copper(II) lattice. The Cu^{II} atom has a square pyramidal geometry with four $btaO^-$ ligands at the basal plane. The $btaO^-$ ion functions as a bidentate bridging ligand, with N(3) and the deprotonated oxygen being the ligating atoms. Dc and ac magnetic susceptibility measurements, together with low-field (10 G) and high-field (up to 5000 G) magnetization data, are consistent with ferromagnetic interactions on the scale of the crystal lattice with two critical temperatures: 6.4 and 4.4 K. The former critical temperature could correspond to a transition from a paramagnetic to a ferromagnetic state; the latter one, to a transition from a ferromagnetically ordered state to its 3D ordering. The magnetic data, along with the field dependence of the magnetization and the EPR data, are also in line with a soft magnet. Moreover, the EPR studies performed on **4** reveal unique features reported for the first time in the field of molecular magnetism.

Introduction

Over the last several years, we and others have been developing the coordination chemistry of benzotriazole (btaH, **I**) and its derivatives.[1−4] One reason for this is the anticorrosion action of btaH and ring-substituted benzotriazoles toward certain metals, particularly copper and its alloys.[5] Chemical, physical, and structural studies on realistic model complexes are needed to understand the complex surface chemistry that leads to corrosion inhibition and to create new inhibitors more efficient than btaH. Another reason is the observation that the reactions between metal β-diketonates or carboxylates and btaH or its ring-substituted (with nondonor groups) derivatives (RbtaH) lead to incomplete replacement of the β-diketonates or carboxylates

[†] Deceased on December 8, 1999.

(1) (a) Reedijk, J.; Roelofsen, G.; Siedle, A. R.; Spek, A. L. *Inorg. Chem.* **1979**, *18*, 1947. (b) Himes, V. L.; Mighell, A. D.; Siedle, A. R. *J. Am. Chem. Soc.* **1981**, *103*, 211. (c) Boyd, P. D. W.; Martin, R. L. *J. Chem. Soc., Dalton Trans.* **1981**, 1069. (d) Hendriks, H. M. J.; Birker, P. J. M. W. L.; Verschoor, G. C.; Reedijk, J. *J. Chem. Soc., Dalton Trans.* **1982**, 623. (e) Kokoszka, G. F.; Baranowski, J.; Goldstein, C.; Orsini, J.; Mighell, A. D.; Himes, V. L.; Siedle, A. R. *J. Am. Chem. Soc.* **1983**, *105*, 5627. (f) Reedijk, J.; Siedle, A. R.; Velapoldi, R. A.; Van Hest, J. A. M. *Inorg. Chim. Acta* **1983**, *74*, 109. (g) Søtofte, I.; Nielsen, K. *Acta Chem. Scand.* **1984**, *A38*, 253. (h) Bencini, A.; Gatteschi, D.; Reedijk, J.; Zanchini, C. *Inorg. Chem.* **1985**, *24*, 207. (i) Moore, D. S.; Robinson, S. D. *Adv. Inorg. Chem.* **1988**, *32*, 171. (j) Olby, B. G.; Robinson, S. D.; Hursthouse, M. B.; Short, R. L. *J. Chem. Soc., Dalton Trans.* **1990**, 621.

(2) (a) Handley, J.; Collison, D.; Garner, C. D.; Helliwell, M.; Docherty, R.; Lawson, J. R.; Tasker, P. A. *Angew. Chem., Int. Ed. Engl.* **1993**, *32*, 1036. (b) Murrie, M.; Collison, D.; Garner, C. D.; Helliwell, M.; Tasker, P. A.; Turner, S. S. *Polyhedron* **1998**, *17*, 3031.

(3) (a) Plakatouras, J.; Perlepes, S. P.; Mentzafos, D.; Terzis, A.; Bakas, T.; Papaefthymiou, V. *Polyhedron* **1992**, *11*, 2657. (b) Diamantopoulou, E.; Zafiropoulos, Th. F.; Perlepes, S. P.; Raptopoulou, C. P.; Terzis, A. *Polyhedron* **1994**, *13*, 1593. (c) Plakatouras, J. C.; Bakas, T.; Huffman, C. J.; Huffman, J. C.; Papaefthymiou, V.; Perlepes, S. P. *J. Chem. Soc., Dalton Trans.* **1994**, 2737. (d) Skorda, K.; Bakalbassis, E. G.; Mrozinski, J.; Perlepes, S. P.; Raptopoulou, C. P.; Terzis, A. *J. Chem. Soc., Dalton Trans.* **1995**, 2317.

10.1021/ic991149i CCC: $19.00
Published on Web 05/23/2000

by the deprotonated benzotriazoles and large heteroleptic 3d metal arrays with novel structural motifs and interesting magnetic properties.[2,4] For example, in recent reports,[4b,c] we have shown that the systematic investigation of the [Ni(β-diketonate)$_2$L$_2$]/RbtaH reaction mixture leads to three families of high-nuclearity complexes: $[Ni_5(OH)(acac)_4(Rbta)_5(H_2O)_4]$ (**1**), $[Ni_5(dbm)_4(Rbta)_6(MeCO_2)_4]$ (**2**), and $[Ni_9(bzac)_6(Rbta)_{12}(MeOH)_6]$ (**3**) (L = H_2O, EtOH; acacH = acetylacetone; dbmH = dibenzoylmethane; bzacH = benzoylacetone; RbtaH = 5-methyl-, 6-methyl-, 5,6-dimethyl-, and 5-chlorobenzotriazole). Clusters belonging to families **1**−**3** possess the intermediate-spin ground states [$S = 0$, $S = 1$], [$S = 1$, $S = 2$], and [$S = 2$, $S = 3$], respectively. Thus, the benzotriazolate ligands have been among the important players in the field of polynuclear transition metal chemistry.

More recently, our efforts have turned toward the use of benzotriazoles substituted on the azole ring with donor groups to see how incorporation of this ligand type might affect the structures and physical properties of the products. The first ligand employed was 1-hydroxybenzotriazole (btaOH, **II**), a well-known peptide-coupling additive.[6] In the present work, reactions of $[Cu_2(O_2CMe)_4(H_2O)_2]$ with btaOH were investigated; these studies resulted in the isolation of the three-dimensional (3D) polymeric complex $[Cu(btaO)_2(MeOH)]_n$ (**4**), which exhibits interesting structural and magnetic characteristics.

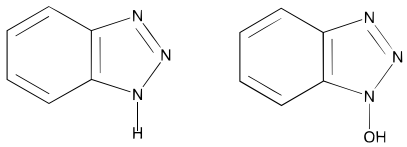

I, btaH **II, btaOH**

Transition metal coordination polymers are of considerable interest as magnetic, electronic, and photooptical materials.[7] In particular, the preparation and characterization of molecule-based materials which exhibit cooperative magnetic interactions, i.e., ferro- or ferrimagnetic behavior, are a growing area of interdisciplinary research. In this context, the design of multi-dimensional structures finds applications in the field of molecular magnets to obtain materials with sufficiently high ordering temperatures.[8,9]

Experimental Section

Materials. All manipulations were performed under aerobic conditions using materials as received (Aldrich). Methanol was distilled before use.

Physical Measurements. C, H, and N analyses were conducted by the microanalytical service of University of Ioannina, Greece. Copper analysis was carried out by EDTA titration. Infrared spectra (4000−500 cm^{-1}) were recorded on a Perkin-Elmer 16 PC infrared spectrometer with samples prepared as KBr pellets. Solid-state (diffuse reflectance, 800−300 nm) electronic spectra were recorded on a Varian Cary 3 instrument. Thermogravimetric (TG), differential thermogravimetric (DTG), and differential thermal analysis (DTA) data were obtained on a Seiko 200 TG/DTA instrument in a dinitrogen gas flow (50 cm^3 min^{-1}); a sample weight of 5 mg and a heating rate of 5 °C min^{-1} were used. Magnetic susceptibility measurements were carried out with a Quantum Design MPMS-5S SQUID magnetometer, working in both the dc and ac modes between 2 and 300 K and from 0 to 50 kG. In the dc mode the field-cooled magnetizations (FCMs) were measured upon cooling the sample within a field of 20 G. The raw susceptibility data were corrected for the core diamagnetism estimated from Pascal's constants. Solid-state EPR spectra were recorded on a Bruker ER 200D-SRC X-band spectrometer, equipped with an Oxford ESR 9 cryostat, in the temperature range 295−4.2 K. A Bruker E-236 bimodal cavity was used to generate the microwave magnetic fields $B_1 \| B$ and $B_1 \perp B$. The frequencies were approximately 9.6 GHz for the vertical mode and 9.4 GHz for the parallel mode. X-ray powder diffraction data were collected with a Siemens D500 diffractometer employing Cu Kα radiation and a secondary-beam graphite monochromator, where the aperture and the soller slits were set at 1.0°.

Safety Note! *Benzotriazoles and benzotriazolate complexes are potentially explosive, and caution should be exercised in handling such compounds*. However, the small quantities used in this study were not found to present a hazard.

$[Cu(btaO)_2(MeOH)]_n$ (4). To a stirred, hot blue-green solution of $[Cu_2(O_2CMe)_4(H_2O)_2]$ (0.80 g, 2.0 mmol) in MeOH (120 mL) was added a warm solution of btaOH·H_2O (1.22 g, 8.0 mmol) in the same solvent (40 mL). Precipitation of a light green solid began almost immediately. Addition of concentrated aqueous ammonia, 25% (0.7 mL, 9.3 mmol), caused the rapid formation of a deep green solution and dissolution of the solid material. The deep green solution rapidly deposited a dark brown-green powder. The reaction mixture was refluxed for 30 min. The flask was left undisturbed at room temperature for 3 weeks, during which all of the powder was transformed into brown-green prismatic crystals (some of them were suitable for X-ray crystallography). The crystals were collected by filtration, washed with MeOH (2 × 10 mL), and dried in air. Yields as high as 80% (1.16 g) were obtained. Anal. Calcd (found) for $C_{13}H_{12}N_6O_3Cu$: C, 42.91 (42.56); H, 3.33 (3.40); N, 23.10 (22.97); Cu, 17.46 (17.01). IR data (KBr pellet; cm^{-1}): 3488 (m), 3054 (w), 2985 (w), 2944 (w), 2840 (w), 1614 (w), 1492 (w), 1446 (m), 1400 (s), 1370 (sh), 1280 (w), 1208 (sh), 1196 (m), 1158 (s), 1132 (w), 1110 (m), 1014 (s), 948 (w), 784 (sh), 774 (sh), 748 (s), 648 (w), 608 (m), 576 (w), 524 (w), 476 (m). Solid-state (diffuse reflectance) electronic spectral data (λ_{max}, nm): 670, 581 (sh), 455, 375, 306. The IR and electronic spectra of the crystals were identical with those of the brown-green powder mentioned above.

X-ray Crystallography. A brown-green prismatic crystal of **4** with approximate dimensions 0.20 × 0.50 × 0.50 mm was mounted in air. Diffraction measurements were made on a $P2_1$ Nicolet diffractometer using Zr-filtered Mo radiation. Complete crystal data and parameters for data collection are reported in Table 1. Unit cell dimensions were determined and refined by using the angular settings of 25 automatically centered reflections in the range $11 < 2\theta < 23°$. Intensity data were recorded using a $\theta-2\theta$ scan to $2\theta(\max) = 56°$ with a scan speed of 3.0°/min and a scan range of 2.5° plus the $\alpha_1\alpha_2$ separation. Three

(4) (a) Bakalbassis, E. G.; Diamantopoulou, E.; Perlepes, S. P.; Raptopoulou, C. P.; Tangoulis, V.; Terzis, A.; Zafiropoulos, Th. F. *J. Chem. Soc., Chem. Commun.* **1995**, 1347. (b) Tangoulis, V.; Raptopoulou, C. P.; Terzis, A.; Bakalbassis, E. G.; Diamantopoulou, E.; Perlepes, S. P. *Inorg. Chem.* **1998**, *37*, 3145. (c) Tangoulis, V.; Diamantopoulou, E.; Bakalbassis, E. G.; Raptopoulou, C. P.; Terzis, A.; Perlepes, S. P. *Mol. Cryst. Liq. Cryst.* **1999**, *335*, 463.

(5) (a) Merk. L. E. *Stud. Conserv.* **1981**, *26*, 73. (b) Schmitt, G. *Br. Corros. J.* **1984**, *19*, 165. (c) Sockalingum, D.; Fleischmann, M.; Musiani, M. M. *Spectrochim. Acta, Part A* **1991**, *47*, 1475 and references therein. (d) Fang, B.-S.; Olson, C. G.; Lynch, D. W. *Surf. Sci.* **1986**, *176*, 476 and references therein.

(6) König, W.; Geiger, R. *Ber. Dtsch. Chem. Ges.* **1970**, *103*, 788, 2024, 2034.

(7) See, for example: Denti, G.; Serroni, S.; Campagna, S.; Juris, A.; Ciano, M.; Balzani, V. In *Perspectives in Coordination Chemistry;* Williams, A. F., Floriani, C., Merbach, A. E., Eds.; VCH: Weinheim, Germany, 1992; pp 153−164.

(8) (a) *Magnetic Molecular Materials*; Gatteschi, D., Kahn, O., Miller, J. S., Palacio, F., Eds.; Kluwer Academic Publishers: Dordrecht, The Netherlands, 1991. (b) Kahn, O.; Pei, Y.; Journaux, Y. Molecular Inorganic Magnetic Materials. In *Inorganic Materials*, 2nd ed.; Bruce, D. W., O'Hare, D., Eds.; Wiley: New York, 1996; pp 59−114.

(9) (a) Miller, J. S.; Epstein, A. J. *Angew. Chem., Int. Ed. Engl.* **1994**, *33*, 385. (b) Baron, V.; Gillon, B.; Cousson, A.; Mathonière, C.; Kahn, O.; Grand, A.; Öhrström, L.; Delley, B.; Bonnet, M.; Boucherle, J.-X. *J. Am. Chem. Soc.* **1997**, *119*, 3500 and references therein. (c) Escuer, A.; Vicente, R.; Goher, M. A. S.; Mautner, F. A. *Inorg. Chem.* **1997**, *36*, 3440 and references therein. (d) Lloret, F.; De Munno, G.; Julve, M.; Cano, J.; Ruiz, R.; Caneschi, A. *Angew. Chem., Int. Ed. Engl.* **1998**, *37*, 135. (e) Batten, S. R.; Jensen, P.; Moubaraki, B.; Murray, K.; Robson, R. *Chem. Commun.* **1998**, 439.

Table 1. Crystallographic Data for Complex **4**

empirical formula	$C_{13}H_{12}N_6O_3Cu$	V, Å^3	1446.6(3)
fw	363.82	Z	4
space group	$P4_32_12$	ρ_{obsd}, g cm^{-3}	1.650
T, °C	25	ρ_{calc}, g cm^{-3}	1.670
λ, Å	0.710 70	μ(Mo Kα), mm^{-1}	1.54
a, Å	9.915(1)	R1[a]	0.0232
b, Å	9.915(1)	wR2[a]	0.0634
c, Å	14.715(2)		

[a] $w = [\sigma^2(F_o^2) + (aP)^2 + bP]^{-1}$ and $P = (\max(F_o^2, 0) + 2F_c^2)/3$; $a = 0.0415$, $b = 0.4371$. $R1 = \sum(|F_o| - |F_c|)/\sum(|F_o|)$ and $wR2 = [\sum w(F_o^2 - F_c^2)^2/\sum[w(F_o^2)^2]^{1/2}$ for 1603 reflections with $I > 2\sigma(I)$. Absolute structure parameter: $-0.04(2)$.

standard reflections monitored every 97 reflections showed less than 3% fluctuation and no decay. Lorentz, polarization, and ψ-scan absorption corrections were applied using Crystal Logic software.

Symmetry-equivalent data of **4** were averaged with $R = 0.0195$ to give 1745 independent reflections from a total of 2285 collected. The structure was solved by direct methods using SHELXS-86[10a] and refined by full-matrix least-squares techniques on F^2 with SHELXL-93[10b] using 1740 reflections and refining 130 parameters. The carbon atom [C(10)] of the coordinated MeOH sits on a 2-fold symmetry axis, and therefore, O(2) is disordered over two positions and was refined with an occupation factor fixed at 10.5; its hydrogen atom was not found. Of the three hydrogen atoms on C(10), only one was located and refined with 50% occupancy. All hydrogen atoms of the bta$^-$ ligand were located by difference maps and their positions refined isotropically.

All non-hydrogen atoms were refined anisotropically. The final values of R1 and wR2 for observed data are listed in Table 1. The maximum and minimum residual peaks in the final difference map were $+0.280$ and -0.318 e/Å^3. The largest shift/esd in the final cycle was 0.584.

Results and Discussion

Synthesis and Characterization. The reaction of $[Cu_2(O_2CMe)_4(H_2O)_2]$ with 4 molar equiv of btaOH·H_2O and concentrated aqueous NH_3 in MeOH rapidly affords a dark brown-green precipitate of analytically pure $[Cu(btaO)_2(MeOH)]_n$ (**4**) in almost quantitative yield, as evidenced by microanalysis. Storage of the reaction flask at room temperature for 3−4 weeks results in the transformation of the powder into small X-ray-quality crystals of the same color. IR spectra of the crystals and the powder are identical. This preparation can be summarized by eq 1. The same product can be isolated from the

$$n[Cu_2(O_2CMe)_4(H_2O)_2] + 4n\text{btaOH}\cdot H_2O + 4nNH_3 + 2n\text{MeOH} \xrightarrow{\text{MeOH}} \underset{\mathbf{4}}{2[Cu(\text{btaO})_2(\text{MeOH})]_n} + 4nNH_4O_2CMe + 6nH_2O \quad (1)$$

1:3:3 and 1:2:2 $[Cu_2(O_2CMe)_4(H_2O)_2]$/btaOH·H_2O/NH_3 stoichiometries. A second clean route to **4** (not included in the Experimental Section) was also developed by employing methanolic solutions of $Cu(NO_3)\cdot 3H_2O$, btaOH·H_2O, and NaOH as reactants in a 1:2:2 molar ratio. Omission of NH_3 from reaction 1 results in a light green solid whose structural identity has yet to be established but which, on the basis of microanalytical and IR data, appears to have the empirical formula Cu(O$_2$CMe)(btaO)(btaOH); attempts to characterize this material are continuing. Obviously, NH_3 is necessary for the full deprotonation of the ligand. **4** is practically insoluble in all common organic solvents, including DMF and DMSO, due to its 3D polymeric structure (vide infra).

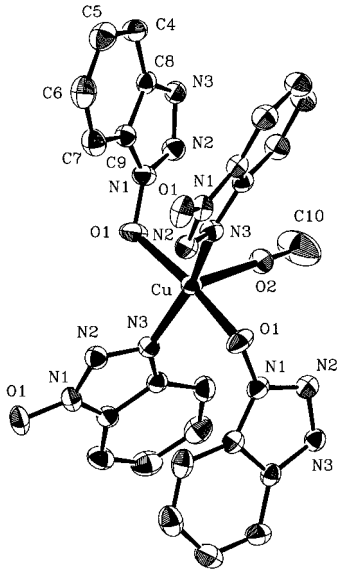

Figure 1. ORTEP view of the coordination sphere of Cu in complex **4**, showing 50% probability ellipsoids and the atom-labeling scheme. Hydrogen atoms have been removed for clarity.

The thermal decomposition data of **4** show a first weight loss in one endothermic step between 80 and 135 °C, which corresponds to the release of the methanol molecule [calcd (found): 8.8% (8.7%)]. The relatively high temperature of MeOH loss indicates that this molecule is coordinated. A clear TG plateau is reached at 140 up to 205 °C, suggesting that the unsolvated compound is thermally stable; this material explodes at 206 °C.

In the IR spectrum, complex **4** exhibits a medium-intensity band at 3488 cm^{-1}, assignable[11] to $\nu(OH)_{\text{coord. MeOH}}$. The strong band at 1014 cm^{-1} is assigned to the C−O stretching vibration of the coordinated methanol molecule.[12] The spectra of the sodium and potassium salts of 1-hydroxybenzotriazole (btaONa, btaOK) exhibit bands at 1180 and ca. 1105 cm^{-1}, associated with the ν(N=N) and ν(N−N) modes of vibration, respectively.[1f] These bands are shifted to 1196 and 1132 cm^{-1}, respectively, in the spectrum of the complex; these shifts to higher frequencies are compatible with N(3) being the donor atom for copper(II).[3a,b] The ν(N−O) bands of btaOH·H_2O and btaOK are at 1224 and 1190 cm^{-1}, respectively. The 1224 cm^{-1} band is shifted to a lower wavenumber (1158 cm^{-1}) upon coordination of the deprotonated oxygen to copper(II).[13]

The solid-state UV/visible spectrum of **4** exhibits three CT transitions in the 455−306 nm range and two d−d transitions at lower energies. The d−d spectrum of the complex is characteristic of its five-coordinate square pyramidal structure with the CuN_2O_3 chromophore.[14−16] The spectrum exhibits maxima at 581 and 670 nm, which are assigned to $B_1 \rightarrow E$ and $B_1 \rightarrow B_2$ transitions, respectively, in C_{4v} symmetry; the third

(10) (a) Sheldrick, G. M. *SHELXS-86*: *Structure Solving Program*; University of Göttingen: Göttingen, Germany, 1986. (b) Sheldrick, G. M. *SHELXL-93*: *Crystal Structure Refinement*; University of Göttingen: Göttingen, Germany, 1993.

(11) Nakamoto, K. *Infrared and Raman Spectra of Inorganic and Coordination Compounds*, 4th ed.; Wiley: New York, 1986; pp 213, 231.

(12) Quaeyhaegens, F. J.; Perlepes, S. P.; Desseyn, H. O. *Spectrochim. Acta, Part A* **1989**, *45*, 809.

(13) Ruiz, R.; Sanz, J.; Cervera, B.; Lloret, F.; Julve, M.; Bois, C.; Faus, J.; Munoz, M. C. *J. Chem. Soc., Dalton Trans.* **1993**, 1623.

(14) Lever, A. B. P. *Inorganic Electronic Spectroscopy*, 2nd ed.; Elsevier: Amsterdam, 1984; pp 308−314, 356, 565, 568, 569.

(15) Reinen, D.; Friebel, C. *Inorg. Chem.* **1984**, *23*, 791.

(16) Christou, G.; Perlepes, S. P.; Libby, E.; Folting, K.; Huffman, J. C.; Webb, R. J.; Hendrickson, D. N. *Inorg. Chem.* **1990**, *29*, 3657.

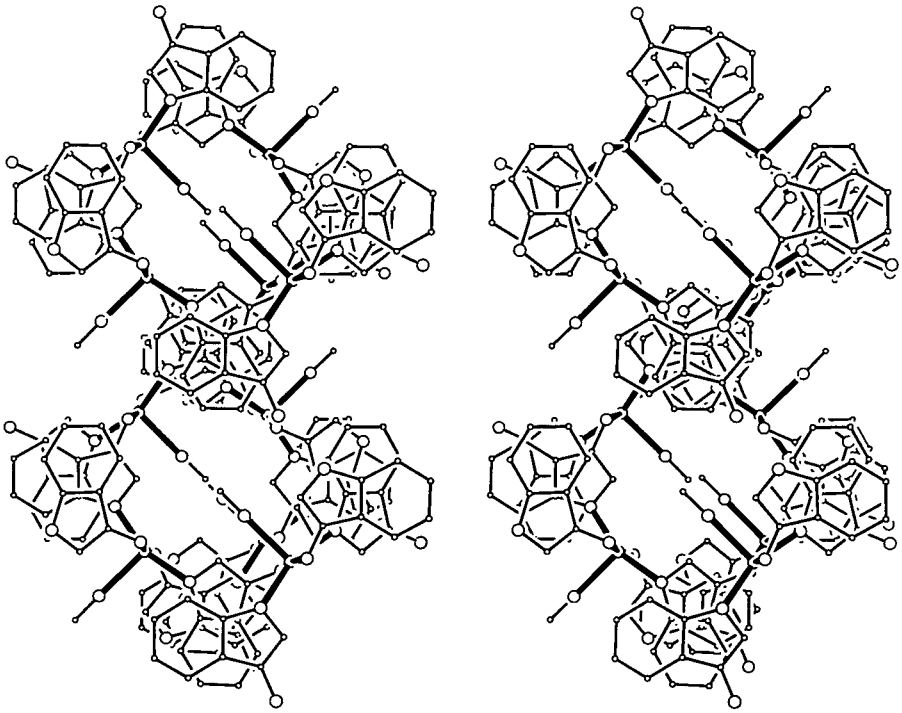

Figure 2. Stereoview showing the helical conformation of **4**.

Table 2. Selected Interatomic Distances (Å) and Angles (deg) for Complex 4[a]

	Distances		
Cu···Cu	6.175(1)	Cu−O(2)	2.333(3)
Cu−O(1)	1.965(1)	N(1)−O(1)	1.331(2)
Cu−O(1)^{i}	1.965(1)	N(1)−N(2)	1.326(2)
Cu−N(3)^{ii}	1.998(2)	N(2)−N(3)	1.331(2)
Cu−N(3)^{iii}	1.998(2)		
	Angles		
O(1)−Cu−O(1)^{i}	170.6(1)	N(3)^{ii}−Cu−O(2)	104.6(1)
O(1)−Cu−N(3)^{ii}	85.1(1)	N(3)^{iii}−Cu−O(2)	96.8(1)
O(1)−Cu−N(3)^{iii}	93.1(1)	N(1)−O(1)−Cu	118.5(1)
O(1)−Cu−O(2)	106.4(1)	N(2)−N(3)−Cu^{iv}	112.6(1)
O(1)^{i}−Cu−O(2)	83.0(1)	C(8)−N(3)−Cu^{iv}	138.4(1)
N(3)^{ii}−Cu−N(3)^{iii}	158.2(1)		

[a] Symmetry transformations used to generate equivalent atoms: (i) $-y+1, -x+1, -z+0.5$; (ii) $x-0.5, -y+1.5, -z+0.25$; (iii) $y-0.5, -x+1.5, z+0.25$; (iv) $-y+1.5, x+0.5, z-0.25$.

$B_1 \rightarrow A_1$transition is expected to appear above the longest wavelength limit (800 nm) of the instrument used.[14,16]

Description of Structure. An ORTEP representation of the coordination sphere of Cu in complex **4** is shown in Figure 1, while a stereoview emphasizing the helical conformation of the complex is provided in Figure 2. Selected interatomic distances and angles are collected in Table 2.

4 is a 3D coordination polymer. The Cu^{II} ion displays a square pyramidal coordination with four btaO$^-$ ligands on the basal plane (vide infra). Two of these ligands, in trans positions, are coordinated through N(3), and the other two, through O(1). Each btaO$^-$ ligand bridges two sequential metal ions through its O(1) and N(3) atoms. The structure is built up with helices down the *c* axis with the 2_1 screw as the axis of the helix, each unit cell "containing" two helices. The repeat unit of the helix is [(btaO)N3−Cu−N3′(btaO)O1-Cu′−O1′-]. The Cu^{II} ions exhibit a tetrahedral arrangement of four five-coordinate metal ions centered on a fifth, resulting in the formation of a diamond-like framework. The basal plane of the square pyramid of the central copper in this tetrahedron—containing its magnetic orbital (vide infra)—is perpendicular to each one of its four neighbors (see Figure 2). Each helix has four closest-neighboring helices along the $a+b$ axes through the btaO$^-$ portions of the repeat unit and four next neighbors along the *ab* diagonals through the N3−Cu−N3′ and O1−Cu−O1′ portions of the repeat unit. There is also a 4_3 screw axis going through the btaO$^-$ units.

The Cu−N distance of 1.998(2) Å is within the normal range observed for other structurally characterized copper(II)−benzotriazole complexes.[2,3d] The metal coordination geometry is best described as distorted square pyramidal with the methanol oxygen atom [O(2)] at the apex. Analysis of the shape-determining angles using the approach of Addison, Reedijk, and co-workers[17] yields a value for the trigonality index, τ, of 0.21 for the copper ($\tau = 0$ and 1 for perfect square pyramidal and trigonal bipyramidal geometries, respectively). As expected, the axial bond [2.333(3) Å] is the longest. Cu lies 0.272(1) Å above the O(1), O(1)[$-y+1, -x+1, -z+0.5$], N(3)[$x-0.5, -y+1.5, -z+0.25$], N(3)[$y-0.5, -x+1.5, z+0.25$] least-squares plane (maximum deviation of 0.129(1) Å for N(3)[$y-0.5, -x+1.5, z+0.25$]) toward O(2). The distance O(2)···N(2) [$-y+1, -x+1, -z+0.5$] is 2.906(2) Å, possibly indicating a weak intermolecular H-bonding interaction.

Dc Magnetic Susceptibility. The magnetic behavior of **4**, in the form of the χ_M versus T plot within a field of 1000 G, is shown in Figure 3. At room temperature, $\chi_M T$ is equal to 0.434 $cm^3\ mol^{-1}$ K, as expected for a noncoupled copper(II) ion with $g = 2.15(1)$. When the temperature is lowered, $\chi_M T$ increases, and around $T = 6$ K the increase becomes quite abrupt, reaching a value of 15.83 $cm^3\ mol^{-1}$ K at 4.5 K, which is about 35 times as large as expected for a noncoupled copper(II) compound. From that temperature down to 3 K, the product decreases, reaching a value of 11.83 $cm^3\ mol^{-1}$ K. The temperature variation of the inverse of χ_M follows the Curie−Weiss law with Curie and Weiss constants of C=0.42(1) $cm^3\ mol^{-1}$ and $\Theta = 8.35(5)°$, respectively. In an attempt to explore the nature of the magnetic ordering, various types of magnetic measurements were performed and will be discussed below.

(17) Addison, A. W.; Rao, T. N.; Reedijk, J.; Rijn, J.; Verschoor, G. C. *J. Chem. Soc., Dalton Trans.* **1984**, 1349.

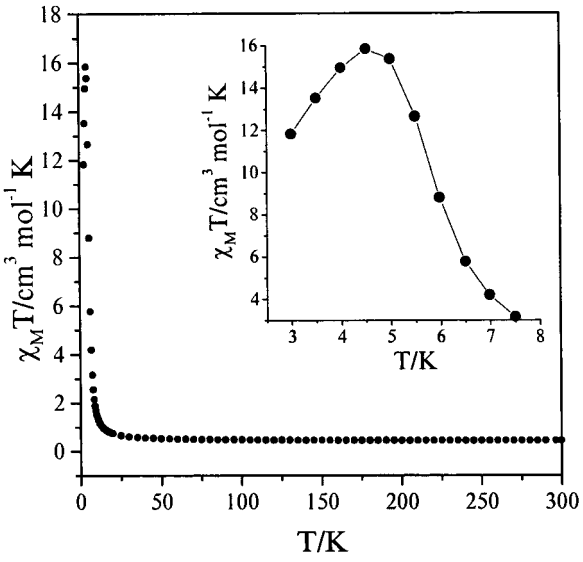

Figure 3. Plot of $\chi_M T$ versus T for a polycrystalline sample of **4** in an applied magnetic field of 1000 G. In the inset, the low-temperature (3−8 K) behavior of $\chi_M T$ is shown, where a peak at 4.5 K is clearly seen.

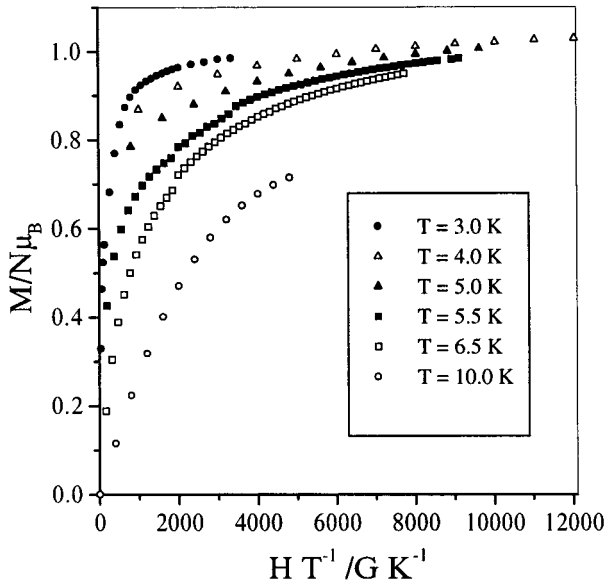

Figure 4. Isothermals of magnetization of **4** in the field range H = 0−5 T.

XRD Measurements. An X-ray powder diffraction spectrum was recorded to check the crystallinity of the sample used for the magnetic measurements. By the Rietveld method,[18] it was confirmed that the sample was the polycrystalline form of complex **4**.

Magnetization Measurements. The isothermals of the variation of the magnetization M versus HT^{-1}, where the applied magnetic field H varies from 0 to 50000 G at various temperatures from 3 to 10 K, are shown in Figure 4. The transition from a ferromagnetically ordered state (3−6 K) to a paramagnetic state (T = 10 K), where the Brillouin character of the magnetization curve appears, is quite clear. The isothermal of magnetization at 3 K clearly shows that the magnetization reaches the saturation value expected for a copper(II) compound (1.05 $N\mu_B$) in an abrupt fashion at 4000 G. This indicates that a low field of 4000 G is sufficient to align all the local spins along the direction of the field.

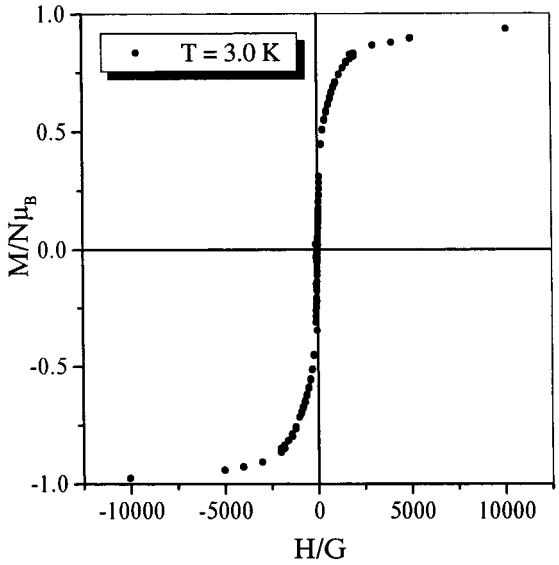

Figure 5. Hysteresis loop for a powdered sample of **4** at 3 K.

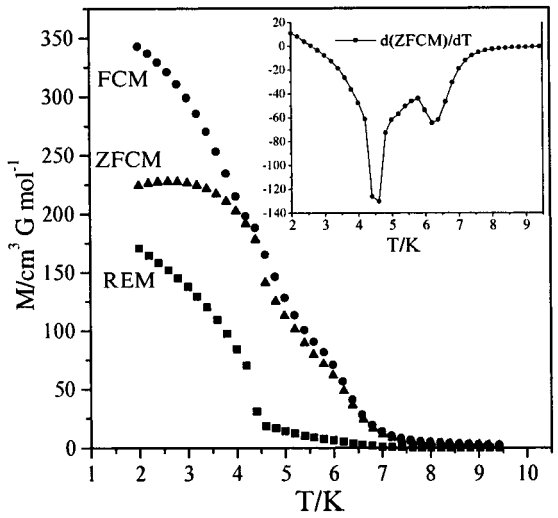

Figure 6. Temperature dependence of the field-cooled magnetization (FCM), zero-field-cooled magnetization (ZFCM), and remnant magnetization (REM) of **4** in an applied field of 10 G. The derivative of the zero-field-cooled magnetization data is shown in the inset.

Hysteresis Loop. The field dependence of the magnetization at 3 K is shown in Figure 5. As expected for a magnet, the zero-field suceptibility is close to infinite and the saturation magnetization is reached under a weak field, about 4000 G. No coercivity was observed. The compound may be considered as a soft magnet.

FCM, ZFCM, and REM Measurements. The temperature dependences of the field-cooled magnetization (FCM), zero-field-cooled magnetization (ZFCM), and remnant magnetization (REM) in the dc mode within an applied field of 10 G in the 2−10 K temperature range are shown in Figure 6. The FCM recorded on cooling the sample within a field of 5 G shows a break below 7 K, with two inflection points at 6.4 and 4.4 K, the latter being more pronounced than the former. The ZFCM recorded on cooling the sample to 2 K in zero field and then warming the sample within a field of 10 G is below the FCM up to 4.4 K. At this temperature, FCM and ZFCM essentially merge. In the inset of Figure 6, the derivative of ZFCM is shown, where the two peaks at 4.4 and 6.4 K are clearly

(18) Wiles, D. A.; Young, R. A. *J. Appl. Crystallogr.* **1981**, *14*, 149.

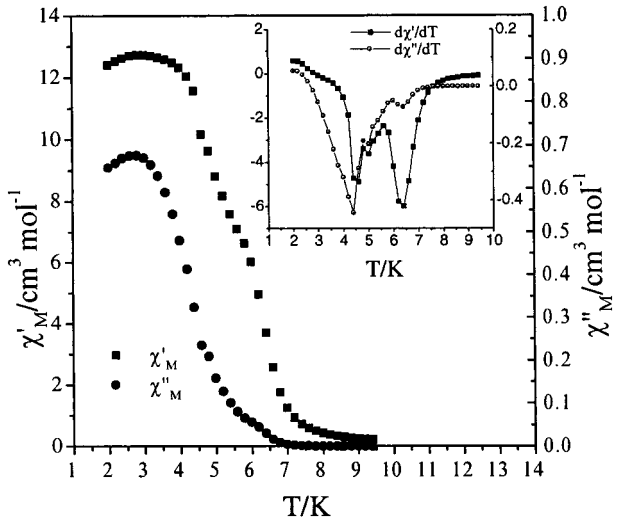

Figure 7. Temperature dependence of the in-phase, χ'_M, and out-of-phase, χ''_M, ac magnetic susceptibilities of **4**. In the inset, the derivatives of χ'_M and χ''_M are plotted to present the cusplike peaks.

resolved. The REM recorded upon warming in zero field a sample cooled within a field of 10 G shows a break and almost vanishes at 4.4 K. The residual REM vanishes only at 6.4 K. Analogous measurements (see Supporting Information) performed at higher excitation fields (1000 G) showed a break around 6 K without any other inflection points. From 5 to 10 K, the two curves (FCM and ZFCM) coincide, while from 2 to 5 K the ZFCM is below the FCM. The REM is very small, close to zero at 1000 G. This means that the critical temperature moves to lower values as the excitation field increases, which is not unusual,[19] while the second inflection point at 4.4 K disappears.

Ac Magnetic Susceptibility. The temperature dependences of the in-phase, χ'_M, and out-of-phase, χ''_M, ac magnetic susceptibilities are presented in Figure 7. χ'_M shows a break below 7 K, with two inflection points at 6.4 and 4.4 K. χ''_M is zero down to ca. 7 K and then also exhibits two inflection points, around 6.4 and 4.4 K, the latter being again more pronounced than the former. These cusplike peaks are shown in the inset of Figure 7, where the derivatives of χ'_M, and χ''_M are plotted, and are unusual, considering the very sharp peaks of other molecular ferromagnets. These peaks will be discussed extensively in the next section.

It emerges from these magnetic data that the compound exhibits a complicated long-range ferromagnetic ordering with two transition temperatures, namely 4.4 and 6.4 K. Therefore, from the start, the interpretation of the magnetic data in such a complex system is difficult.

Magnetic Properties: Discussion. The mechanism of how many-body systems come to reduce their free energy by ordering is difficult to determine when (a) the fundamental interactions compete with each other, (b) randomness occurs (e.g., in positions of spins or in signs of neighboring coupling), (c) disorder exists (e.g., in a lattice site or bond), and (d) frustration, arising from a combination of randomness and mixed exchange interactions, characterizes their magnetic behavior. It is very likely that, in our case, a magnetic anisotropy exists which is purely geometrical in origin. This will be discussed in more detail directly below.

As was shown above, the magnetic ions in **4** are situated at the corners of a three-dimensional, diamond-like network of corner-sharing distorted tetrahedra. The distortion in each particular tetrahedron is shown in Chart 1.

Chart 1. Angles in Each Tetrahedron of **4**

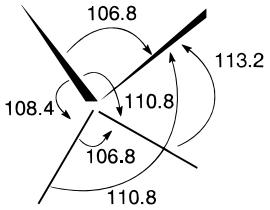

Chart 2. Views of the 3D Diamond-like Cu(II) Network of **4**: Top, Slightly Distorted Diamond-like Network; Bottom, Dissimilarity of Exchange Interactions in the Same Network

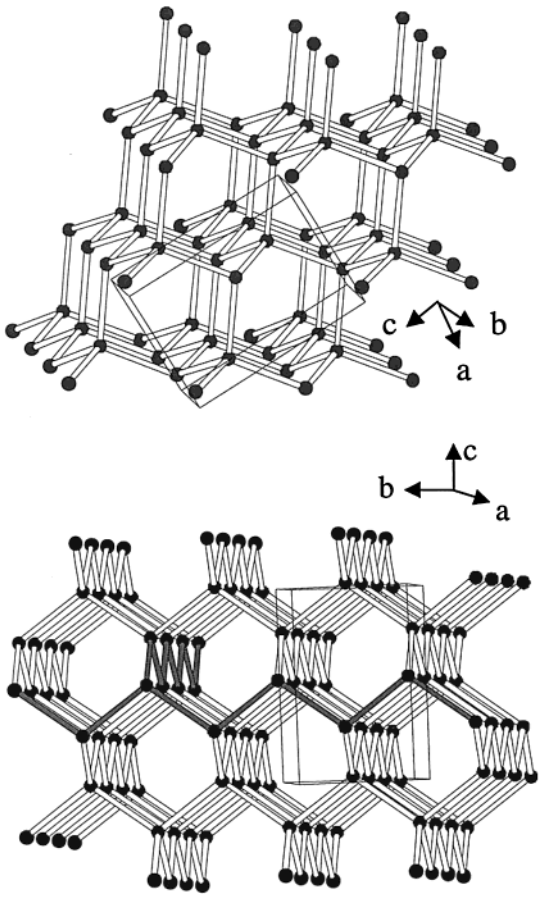

All angles refer to $Cu_{outer}-Cu_{central}-Cu_{outer}$. Considering the topology of the other four neighboring copper(II) tetrahedra, sharing a different corner with this one, it is clear that there is no unique preferred vector spin alignment satisfying fully all four equivalent ferromagnetic interactions. The distance between the central Cu^{II} ion and the four peripheral ones at the corners of each tetrahedron is 6.025 Å. The distance between the outer Cu^{II} ions is 9.135 Å. The ligation between the central Cu^{II} ion and the outer ones favors ferromagnetic interactions, while the outer Cu^{II} ions have no direct exchange pathway. In Chart 2, the 3D network of the corner sharing tetrahedra is shown from two points of view. In the upper view, the slightly distorted diamond-like network is shown. This consists of Cu^{II} ions, within the [101] plane, which form tetrahedra with those in the vertical positions of this plane. The other view shows the dissimilarity of the exchange interactions in this network. It is clear that, although the exchange pathway along the *a* and *b* axes is the same (solid lines along *a* and *b*), there is no direct exchange pathway along the *c* axis.

(19) Yosida, K. *Theory of Magnetism*; Springer-Verlag: Heidelberg, Germany, 1996.

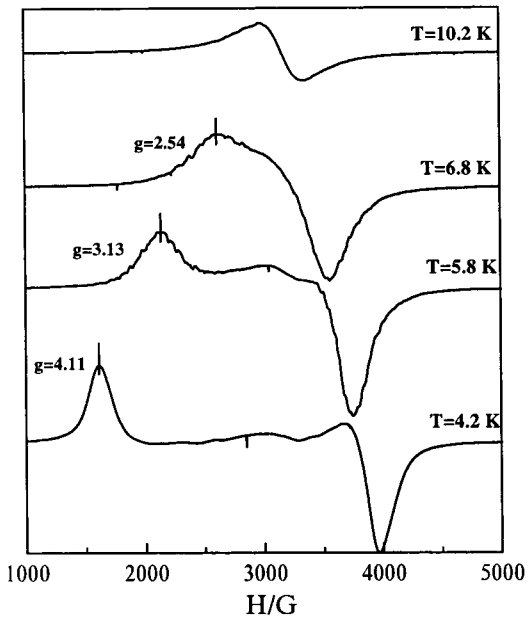

Figure 8. Temperature dependence of the X-band powder EPR spectra of **4** in the 1000−5000 G field range. The microwave field B_1 is peprendicular to the applied field, *B*.

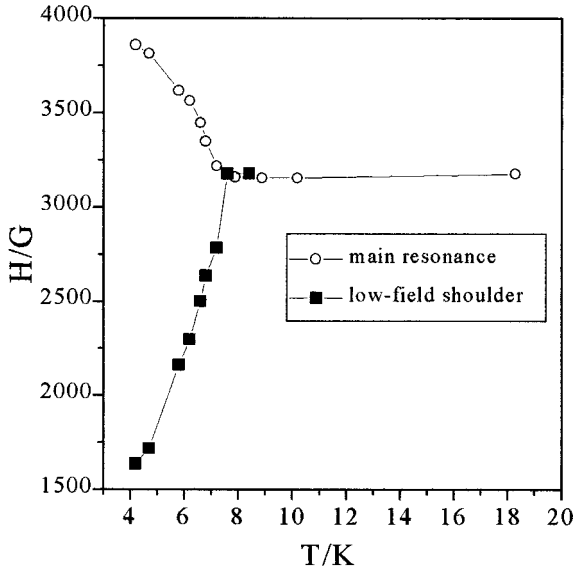

Figure 9. Temperature dependence of the magnetic resonance field for the main features of the EPR spectra of **4** (see text for details).

It is very likely that the previous dissimilarity of the exchange interactions may be reflected in the complex behavior of the magnetic data. In particular, the transition at $T = 6.4$ K possibly corresponds to the phase boundary between the paramagnetic and ordered states in the extended 3D network of the diamond-like structure of **4**. This is due to the main interaction, which is applicable only in the *ab* planes (Chart 2). The second transition at $T = 4.4$ K could be the result of the anisotropy in the exchange interactions. At this temperature, the *ab* planes interact ferromagnetically and the 3D ordering is achieved.

The ac susceptibility of **4** was measured in a 100 G ac field and a zero dc field for frequencies ranging from 5 to 1000 Hz. No frequency dependence was observed, and spin-glass behavior should be excluded for **4**.

EPR Properties: Perpendicular B_1 Orientation. The temperature dependence of the X-band powder EPR spectrum of **4** is shown in Figure 8. While the spectrum at 10 K shows a single, asymmetric resonance centered at $g = 2.13(1)$, new features appear as the temperature is lowered to 4 K. In particular, at the T_c and below that temperature, a shoulder of the main resonance appears, which is continuously shifted toward lower fields ($g = 2.54$ at 6.8 K, $g = 4.11$ at 4.2 K). A second shoulder of the main resonance appears around 5.8 K at 3100 G, remaining unshifted down to 4.2 K. Another dramatic change is the concomitant shift of the main resonance to higher magnetic fields.

The temperature dependence of the g_{eff} values reveals that the anisotropy of the g_{eff} value increases upon magnetic ordering, and thus, the system behaves as an axially anisotropic powdered material.[20] It is worth mentioning that, while similar behavior was reported for $(rad)_2Mn_2[Cu(opba)]_3(DMSO)_2{\cdot}2H_2O$[21] ($rad^+$ = the radical cation of 2-(1-methylpyridinium-4-yl)-4,4,5,5-tetramethylimidazoline-1-oxyl 3-oxide; $opba^{4-}$ = *o*-phenylenebis(oxamato))—for which, however, the low-field shoulder was only shifted by ca. 200 G in the 15−4.2 K temperature range—the simultaneous shift of both the main resonance and its low-field shoulder shown by **4** is reported here for the first time. Another explanation of the new features in the EPR spectrum, in the magnetically ordered state, is the coexistence of different phenomena, which will be discussed below.

Considering the temperature dependence of the low-field feature, a possible explanation could be that, for a given value of the applied field,[22] the magnetization, and therefore the field induced by the magnetization, H_{loc} (local field in the magnetically ordered state), increases as the temperature decreases. In this way, the resonance should be considered not for a unique, H_0, value but for a whole field, ranging from $H_0 - H_{loc}$ to H_{loc}; it follows that $H_0 - H_{loc}$ decreases as T decreases. In our case, this picture, however, is not reflected in the main resonance. This could, in turn, mean that a second phenomenon of ferromagnetic resonance also takes place, which is quite different from that already stated above. The observed dramatic g shift from 2.13(1) to 1.73(1) (see Figure 8) might be due to a short-range effect, reflecting the interconnection of the two ferromagnetic resonances. This complicated behavior of the EPR spectra further supports the hypothesis of the two transition points, already presented in the magnetic discussion.

Figure 9 shows the complicated temperature dependence of both the low-field shoulder and the main resonance. The quantitative interpretation of spectra in the ferromagnetic state is a difficult task, and to the best of our knowledge, the present study is the first in which two different types of ferromagnetic resonances[23] are discussed. It could be also stated here that the difference between the spectrum of $(rad)_2Mn_2[Cu(opba)]_3(DMSO)_2{\cdot}2H_2O$ and ours lies in the topology of the magnetic ions. Moreover, the simplicity of the system (the only magnetic ion is the Cu^{II} ion) makes it a very important candidate for further theoretical investigation. To fully explore the complicated EPR characteristics, single-crystal EPR measurements would be very informative.

Quantum-Chemical Interpretation of the Exchange Mechanism. It was shown above that each Cu^{II} ion displays a square

(20) We thank one reviewer for stimulating comments concerning this point.
(21) Stumpf, U. O.; Ouahab, L.; Pei, Y.; Bergerat, P.; Kahn, O. *J. Am. Chem. Soc.* **1994**, *116*, 3866.
(22) At T_c and below, the field experienced by each magnetic center is $H = H_{ext} + H_{loc}$.
(23) (a) Phaff, A. C.; Swuste, C. H. W.; de Jonge, W. J. M.; Hoogerbeets, R.; van Duyneveldt, A. J. *J. Phys. Chem.* **1984**, *17*, 2583. (b) Hoogerbeets, R.; van Duyneveldt, A. J.; Phaff, A. C.; Swuste, C. H. W.; de Jonge, W. J. M. *J. Phys. Chem.* **1984**, *17*, 2595 and references therein.

pyramidal coordination, with two O(1) and two N(3) atoms in the trans positions of the basal plane, respectively; a methanol oxygen atom occupies the apical position. Due to the longer Cu−O distance of this bond—compared to the others in the coordination sphere of each Cu^{II} ion—the unpaired electron of the Cu^{II} ion occupies a d-type magnetic orbital pointing toward the four nearest neighbors in the basal plane, i.e., the O(1), O(1), N(3), and N(3) atoms. This magnetic orbital is roughly perpendicular (dihedral angle of 77.3°) to the plane of the bridging benzotriazolato ligand—ligation through the O(1) atom—and this is also the case (dihedral angle of 73.8°) with the plane of the neighboring magnetic orbital—ligation through the N(3) atom. Moreover, in the Cu_5 tetrahedral arrangement, each magnetic orbital is perpendicular to each one of its four neighboring magnetic orbitals (see also Figure 2). Thus, the two sequential magnetic orbitals are accidentally orthogonal[24] to each other, because both have the same symmetry and their planes are perpendicular to each other (dihedral angle of 89.4°). The accidental orthogonality of the magnetic orbitals could account well for a ferromagnetic interaction between any two neighboring copper(II) magnetic centers, in close agreement with the experimental magnetic results for **4**.

Conclusions

The initial use of the $btaO^-$ ligand in transition metal chemistry has provided access to a 3D copper(II) complex with interesting structural and magnetic characteristics. In **4**, the $btaO^-$ ion acts as a bidentate bridging ligand. From this study and recent work in our groups, it is clear that the nature of btaOH and its anion makes them versatile new ligands for use with a variety of metals and for a variety of objectives/advantages, including variable denticity levels, 3d−4f mixed-metal chemistry, high-nuclearity aggregate formation and/or linking of the aggregates into polymeric arrays, and ferromagnetic exchange interactions. As far as the magnetic behavior of **4** is concerned, it appears to be both quite interesting and unusual. In particular, its various magnetic susceptibility and magnetization data are consistent with long-range ferromagnetic interactions with two critical temperatures at 6.4 and 4.4 K. The specific EPR studies also reveal quite interesting features.

Acknowledgment. This work was supported by the Greek General Secretariat of Research and Technology (Grant 99ED139 to S.P.P., V.P., and E.G.B. and PLATON Program Grant 1583 to E.G.B.), the Greek Secretariat of Athletics, OPAP (A.T.), and Mrs. Athina Athanassiou (V.T.).

Supporting Information Available: A plot of ZFCM and FCM data recorded within an applied field of 1000 G in the 2−11 K temperature range and an X-ray crystallographic file, in CIF format, for complex **4**. This material is available free of charge via the Internet at http://pubs.acs.org.

IC991149I

(24) Kahn, O. *Molecular Magnetism*; VCH Publishers: New York, 1993; p 163.